Supporting Information

Ha and Boggon 10.1073/pnas.1717437115

SI Materials and Methods

Expression and Purification. PAK4 isoform-2 cDNA (Open Biosystems) encoding 426 aa (UniProt ID: O96013) (residues 1–426, termed $PAK4^{FL}$) was subcloned into a modified pET28 vector (Novagen) with an N-terminal hexa-histidine (6xHis) tag cleavable by tobacco etch virus (TEV) protease. Catalytic domain PAK4 residues 109–426 (termed $PAK4^{cat}$) was subcloned into the same expression vector. Because residues 121–426 of isoform-2 correspond exactly to residues 286–591 in isoform-1, for clarity we discuss kinase domain residues using isoform-1 numbering throughout. We also use isoform-1 numbering for residues in the N terminus (residues 1–119 are identical between isoform-1 and isoform-2). PAK4 residues 1–45 (termed $PAK4^{N45}$) were each subcloned into pMCSG9 vector (SnapGene) which has an N-terminal 6xHis tag followed by maltose binding protein cleavable by TEV protease. Human CDC42 (UniProt ID: P60953) cDNA (a gift of Joseph Schlessinger, Yale University, New Haven, CT) encoding either residues 1–177 or 1–181 was subcloned into pET22b vector (Novagen) with a C-terminal uncleavable 6xHis tag and Q61L mutation. Human RAC1 (UniProt ID: P63000) cDNA (a gift of Ruth Halaban, Yale University, New Haven, CT) encoding residues 1–181 was subcloned into pET22b vector having Q61L mutation with a C-terminal uncleavable 6xHis tag. Mutants were introduced using QuikChange (Agilent Technologies).

$PAK4^{FL}$, $PAK4^{cat}$, and $PAK4^{N45}$ proteins were expressed in BL21-CodonPlus(DE3)RILP (Agilent Technologies) cells by induction with 0.5 mM isopropyl β-D-1-thiogalactopyranoside overnight at 18 °C. Harvested pellets were suspended in lysis buffer [20 mM Tris·HCl, pH 8.0, 100 mM NaCl, 1 mM Tris(2-carboxyethyl)phosphine (TCEP), and 0.1 mM PMSF] and lysed by sonication. The supernatants were affinity-purified by HisTrap chelating column (GE) and then resolved over Resource S (GE) for ($PAK4^{FL}$ or $PAK4^{N45}$) or Resource Q (GE) for ($PAK4^{cat}$, CDC42, or RAC1). Each protein was then loaded to a Superdex 75 10/300GL (GE) column and all elutions indicated monodisperse proteins.

For SAXS, samples of size-exclusion-purified $PAK4^{FL}$ and $PAK4^{FL}$-CDC42 dialyzed against the same buffer (20 mM Tris, pH 8, 300 mM NaCl, and 1 mM TCEP). For ITC, Q61L mutants of CDC42 and RAC1 proteins were preincubated with 5 mM GTP and 10 mM $MgCl_2$ ahead of dialysis. All recombinant proteins were simultaneously dialyzed against the same buffer (PBS, pH 7.4). For kinase assays, following cell lysis proteins were purified by HisTrap chelating column (GE) and dialyzed against 20 mM Tris·HCl, pH 8.0, 150 mM NaCl, and 1 mM DTT.

SAXS. We prepared samples of size-exclusion-purified $PAK4^{FL}$ and $PAK4^{FL}$-CDC42 dialyzed against the same buffer (20 mM Tris, pH 8.0, 300 mM NaCl, and 1 mM TCEP). Final concentrations of 11, 5.6, and 2.8 mg/mL were prepared for $PAK4^{FL}$ and 6.2, 3.1, and 1.5 mg/mL for $PAK4^{FL}$-CDC42. X-ray scattering was conducted at the LiX beamline at the National Synchrotron Light Source II (NSLS-II) and data were collected on a Pilatus 1M detector. Five individual 5-s exposures were collected for each concentration and for a buffer blank. Data integration, averaging, and buffer subtraction was conducted using pyXS (35). Following inspection of each exposure using Primus (36), radiation-damaged exposures were excluded. Exposures were merged together using pyXS and Guinier analysis performed using Primus to calculate R_g. Pair distribution functions $P(r)$ and forward scattering $I(0)$ were calculated using GNOM (37) and molecular weights estimated separately based on Porod volumes calculated in Primus and excluded bead volumes of ab initio models from DAMMIF (38). DAMFILT envelopes were superposed with crystal structures using SUPCOMB (33), but because of the extent of loops unmodeled in the crystal structure no further superposition analyses were conducted. Dimensionless Kratky plots of q_2 vs. $I(q)$, where $q = q \times R_g$ and $I(q) = I(q)/I(0)$, were generated as described (21, 39). Porod–Debye plots of $q^4 \times I(q)$ vs. q^4 were generated as described (21).

Rigid body modeling was conducted using CORAL (40) using the crystal structure of $PAK4^{cat}$-$PAK4^{N45}$-CDC42. Thirty-two unmodeled N-terminal residues include the uncleaved N-terminal His tag sequence "MGSSHHHHHHSSGLVPRGSHMENLYFQGFGK-RKKRVEISAPSNFEHRVHT-GFDQHEQKFTGLPRQWQSLIE-ESAR," there were ninety-two unmodeled PAK4 residues (44–299) (PAK4 isoform 2 used is shorter than isoform 1, so we have maintained the numbering of the kinase domain for consistency with previous catalytic domain structural studies; see ref. 10 for details). Nine unmodeled C-terminal residues of CDC42 include the uncleavable His tag "PPEHHHHHH." Data were cut off at q_{max} = 0.48 $Å^{-1}$. Flexibility analysis conducted by the EOM method (25) used the crystal structure of $PAK4^{cat}$-$PAK4^{N45}$-CDC42. The 92-aa linker was modeled using RANCH and data were cut off at q = 0.25 $Å^{-1}$. Model superpositions were made using SUPCOMB (33).

PAK4 Crystallization and Data Collection.

$PAK4^{FL}$-CDC42 complex. Equal amounts of $PAK4^{FL}$ and $CDC42^{Q61L}$ were mixed together and copurified by Superdex 75 column. The eluted complex was concentrated to 5 mg/mL and incubated with 1 mM phosphoaminophosphonic acid-adenylate ester (AMP-PNP), 1 mM guanylyl imidodiphosphate (GMP-PNP), and 5 mM $MgCl_2$ before setting up crystallization drops. Cocrystals of $PAK4^{FL}$-$CDC42^{Q61L}$ were obtained in 0.1 M Tris·HCl, pH 8.5, 50 mM Na_2SO_4, and 6% (vol/vol) PEG 6,000 at room temperature. The crystals were cryoprotected reservoir buffer plus 25–30% (vol/vol) glycerol. Data were collected at the Advanced Photon Source (APS) beamline 24-ID-E.

$PAK4^{cat}$-$PAK4^{N45}$-CDC42 complex. Separately purified $PAK4^{cat}$, $PAK4^{N45}$, and $CDC42^{Q61L}$ were mixed in a 1:1:1 molar ratio concentrated to 5 mg/mL and incubated with 1 mM AMP-PNP, 1 mM GMP-PNP, and 5 mM $MgCl_2$ before setting up crystallization drops. Cocrystals of $PAK4^{cat}$-$PAK4^{N45}$-$CDC42^{Q61L}$ were grown using hanging-drop vapor diffusion methodology by mixing a 1:1 volume ratio of purified $PAK4^{cat}$-$PAK4^{N45}$-$CDC42^{Q61L}$ and reservoir solution containing 0.1 M Hepes, pH 7.5, and 22% (vol/vol) PEG 1,000 at room temperature. Cryoprotectant buffer contained reservoir buffer plus 25–30% (vol/vol) glycerol. Data were collected at the APS beamline 24-ID-E.

Structure Determination and Refinement.

$PAK4^{FL}$-CDC42 complex. Crystallographic data were processed to 3.0-Å resolution using the HKL2000 package (41). An initial molecular replacement solution was obtained using Phaser (42) using the previously determined crystal structures of PAK4 catalytic domain (PDB ID code 4FIF) (10) and CDC42 (PDB ID code 2ODB) as the search models. This yielded Z-scores for rotation and translation functions of 6.2 and 15.7, respectively, for PAK4 and 3.1 and 9.7 for CDC42. We noted, however, that CDC42 showed poor electron density. Therefore, for refinement we utilized only the coordinates for the PAK4 catalytic domain. We conducted refinement for the PAK4 using Phenix (43), model building in Coot (44), and model quality assessed using MolProbity (45). We then generated electron density maps and confirmed that the molecular

replacement solution for CDC42 correlated well with the unbiased difference density. As CDC42 showed poor electron density that did not allow positional refinement we fixed XYZ coordinates for PAK4 and CDC42. We then set the *B*-factor for CDC42 to the Wilson *B* and conducted one round of grouped *B*-factor refinement for CDC42, resulting in an average *B*-factor for CDC42 of 218.7 $Å^2$ (Table S2). The final *R* and R_{free} values for the $PAK4^{FL}$-CDC42 complex are 25.2% and 30.1%, respectively.

$PAK4^{cat}$-$PAK4^{N45}$-CDC42 complex. Crystallographic data were processed to 2.4-Å resolution using the HKL2000 package (41) and initial phases generated using molecular replacement using Phaser (42) and the previously determined crystal structures of PAK4 catalytic domain (PDB ID code 4FIF) (10) and CDC42 (PDB ID code 2ODB) as the search models. For the $PAK4^{cat}$-$PAK4^{N45}$-$CDC42^{Q61L}$ structure this yielded Z-scores for rotation and translation functions of 8.7 and 6.4, respectively, for $PAK4^{cat}$ and 3.4 and 13.1 for $CDC42^{Q61L}$. Refinement of the $PAK4^{cat}$ and $CDC42^{Q61L}$ was conducted using Refmac5 (46) with a maximum-likelihood target and TLS (translation, libration, screw). Model building was conducted in Coot (44) and during refinement interpretable electron density for $PAK4^{N45}$ became clearly visible, which was built manually. Poor electron density is visible for the β and γ phosphates of AMP-PNP. Model quality assessed using MolProbity (45) yielded final *R* and R_{free} values of 22.1% and 26.4%, respectively. Crystallographic software was compiled by SBGrid (47) and structural figures generated using CCP4mg (48) and PyMOL. Buried surface area was calculated using the PISA server (49). RAC3-PAK4 CRIB (PDB ID code 2OV2) buries 2,028 $Å^2$ and CDC42-PAK6 CRIB (PDB ID code 2ODB) buries an average of 2,108 $Å^2$. A total of 3,152 $Å^2$ are buried between PAK4 and CDC42 in the $PAK4^{cat}$-$PAK4^{N45}$-CDC42 complex.

ITC. For ITC, a Nano-ITC (TA Instruments) was used. Purified proteins following preincubation with 5 mM $MgCl_2$ and 1 mM ATP for $PAK4^{FL}$ or 1 mM GTP for GTPases were simultaneously dialyzed against PBS buffer (pH 7.4) three times. The reference cell was filled with water and the sample cell was filled with PAK4. Protein concentrations were determined using UV. For $PAK4^{FL}$-CDC42 interactions 14 μM of $PAK4^{FL}$ was loaded in the sample cell and either 0.377 mM, 0.187 mM $CDC42^{Q61L}$, or 0.38 mM, 0.189 mM $CDC42^{Q61L/E171R/L174R/E178R}$ was loaded in the syringe. For $PAK4^{FL}$-RAC1 interactions 14 μM of $PAK4^{FL}$ was loaded in the sample cell and 0.312 mM and 0.159 mM $RAC1^{Q61L}$ were loaded in the syringe. For $PAK4^{cat}$ with $PAK4^{N45}$-$CDC42^{Q61L}$ and $PAK4^{cat}$ with $PAK4^{N45}$ interactions 70 μM and 89 μM of $PAK4^{cat}$ was loaded in the sample cell and 0.852 mM and 1.436 mM of $PAK4^{N45}$-$CDC42^{Q61L}$ complex were loaded in the syringe. For $PAK4^{FL\text{-}R489A}$-$CDC42^{Q61L}$ interactions 89 μM of $PAK4^{FL\text{-}R489A}$ was loaded in the sample cell and 0.933 mM, 0.356 mM, and 0.466 mM $CDC42^{Q61L}$ were loaded in the syringe. For $PAK4^{FL\text{-}R489A}$-$CDC42^{Q61L/E171R/L174R/E178R}$ interactions 21 μM of $PAK4^{FL\text{-}R489A}$ was loaded in the sample cell and 0.435 mM and 0.162 mM $CDC42^{Q61L/E171R/L174R/E178R}$ were loaded in the syringe. For $CDC42^{Q61L}$-$PAK4^{N45}$ interactions 93 μM of $CDC42^{Q61L}$ was loaded in the sample cell and 0.898 mM and 0.449 mM of $PAK4^{N45}$ were loaded in the syringe. For $RAC1^{Q61L}$-$PAK4^{N45}$ interactions 92 μM of $RAC1^{Q61L}$ was loaded in the sample cell and 0.449 mM $PAK4^{N45}$ was loaded in the syringe. All ITC experiments were conducted at 25 °C using a stir speed of 350 rpm and incremental titration of 20 injections, 2.5-μL volume, and 300-s intervals. Buffer data (PBS into PBS titration) were subtracted from the corresponding experiment before data fitting. Raw data were processed and integrated with NanoAnalyze software (TA Instruments). The first injection in each experiment was not considered for the analysis. Stoichiometry of interaction (N), dissociation constant (K_d), enthalpy changes (ΔH), and entropy changes (ΔS) were determined using NanoAnalyze software.

In Vitro PAK4 Kinase Assay. Kinase activity was performed using a radioactive with β-catenin as substrate. C-terminal 6xHis-tagged PAK4-FL and its polybasic mutant (R5A and R8A) were purified as described above, and purified CDC42 (1–181, Q61L: constitutive active mutant) and $CDC42^{ELE\text{-}RRR}$ mutant (1–181, Q61L, E171R, L174R, and E178R) were added as effector proteins. Briefly, kinase assays were performed by adding 0.3–0.4 μM of kinase, 2 μM of β-catenin, with/without CDC42/$CDC42^{ELE\text{-}RRR}$, 0.12 μM of cold ATP, and 0.05 μCi of hot [γ33-P] ATP in Tris buffer (20 mM Tris·HCl, pH 8.0, 0.3 M NaCl, 1 mM TCEP, and 10 mM $MgCl_2$), total volume 25 μL. The reaction was conducted at 30 °C for 5 min, 10 min, and 30 min then stopped by addition of 5× sample buffer and analyzed by SDS/PAGE. Dried gels were analyzed by exposure to phosphor storage screen (GE Healthcare) followed by scanning using a Molecular Imager FX Pro Plus System (Bio-Rad) and quantification by optical densitometry Quantity One (Bio-Rad). Relative activities were compared with those measured for PAK4-FL. Measurements were calculated from five independent experiments. Significant differences were calculated by Prism 7 (GraphPad Software) with ANOVA analysis.

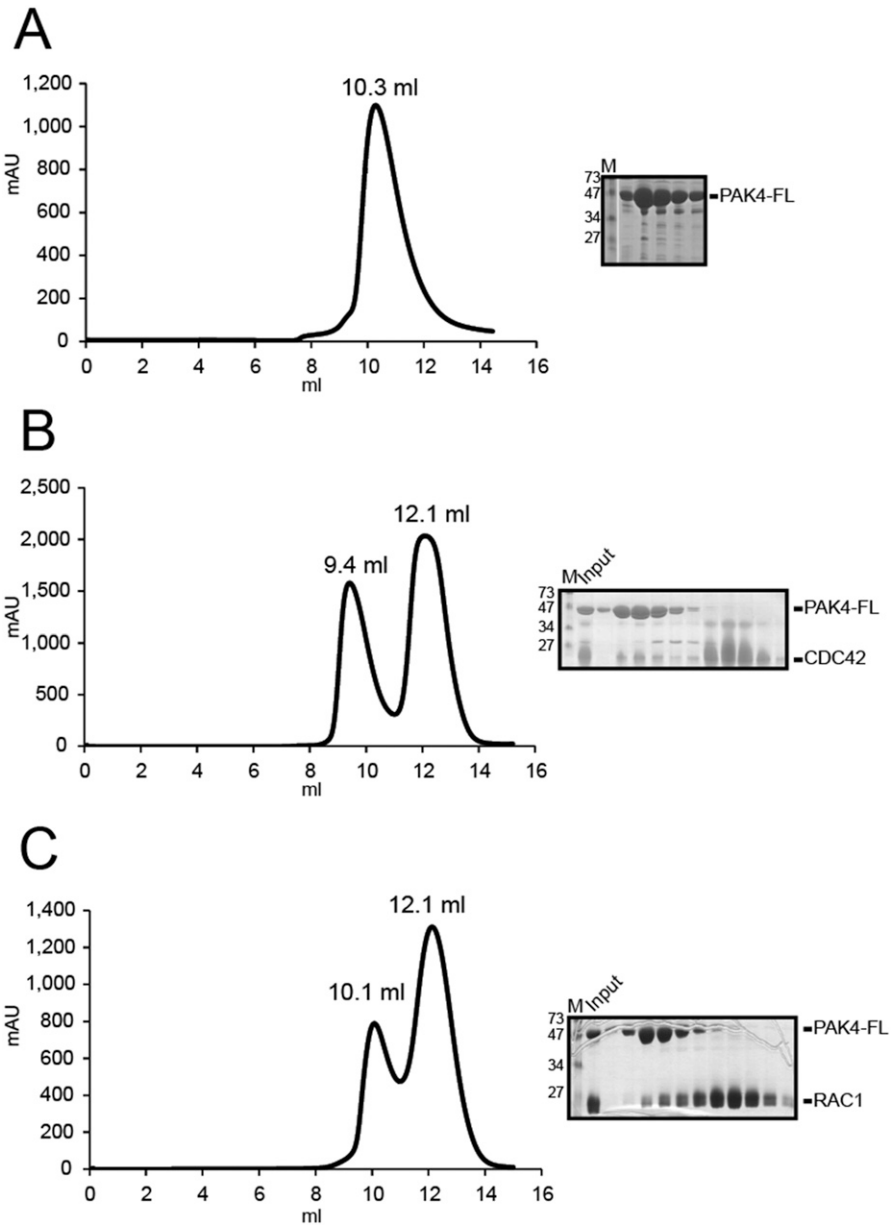

Fig. S1. Gel filtration for PAK4^{FL}, PAK4^{FL} with RAC1, and PAK4^{FL} with CDC42. (*A*) Size-exclusion chromatogram (SEC) showing S75 elution of PAK4^{FL} alone. (*Inset*) Coomassie-stained gel of the peak fraction. (*B*) SEC for mixture of activated CDC42 (Q61L mutant) and PAK4^{FL}. (*C*) SEC for mixture of activated RAC1 (Gln61Leu mutant) and PAK4^{FL}.

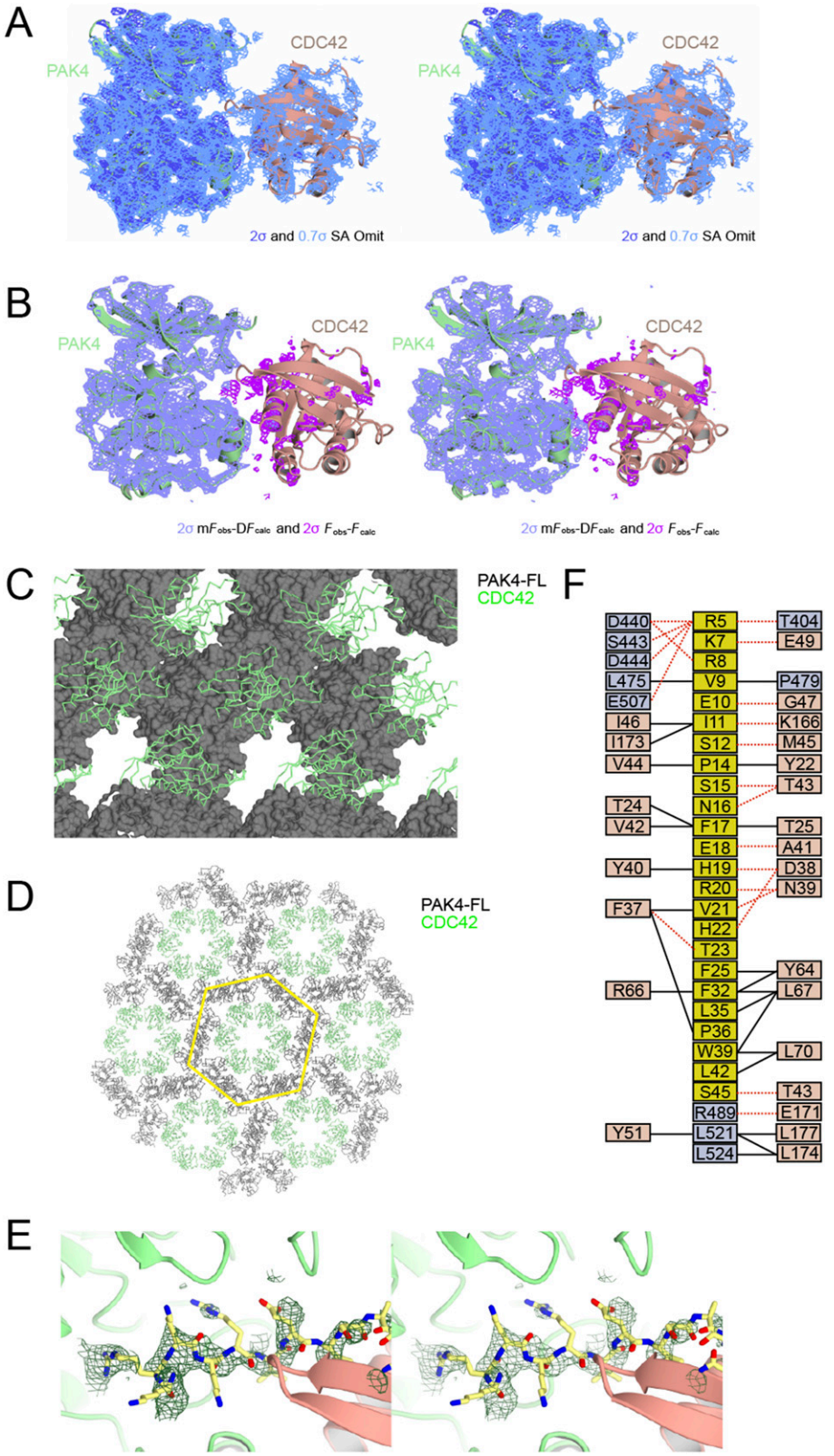

Fig. S2. Structure solution for PAK4^{FL}-CDC42 complex. (*A*) Electron density showing simulated annealed composite omit map (contoured at 2 σ and 0.7 σ) for PAK4^{FL} and CDC42. (*B*) Unbiased mF_{obs} − DF_{calc} (contoured at 2 σ) and F_{obs} − F_{calc} (2 σ) calculated following the molecular replacement solution of just the PAK4 catalytic domain, confirming the placement of CDC42. (*C*) Crystal packing of PAK4 (surface) and CDC42 (ribbon) molecular replacement solution illustrating that CDC42 only makes contact with a single copy of PAK4 within the structure (closest distance to another CDC42 molecule is ∼9 Å). (*D*) Crystal packing of PAK4^{FL} and CDC42. (*E*) Close-up of unbiased F_{obs} − F_{calc} (2.0 σ) showing unsatisfied electron density connecting the kinase substrate binding site and the CRIB binding site. Panel shows electron density from PAK4^{FL}-CDC42 and the superposed final structure of PAK4^{cat}-PAK4^{N45}-CDC42. (*F*) Schematic diagram showing the residues of PAK4 and CDC42 that interact. Dashed line indicates salt bridges and solid line shows nonbonding contacts.

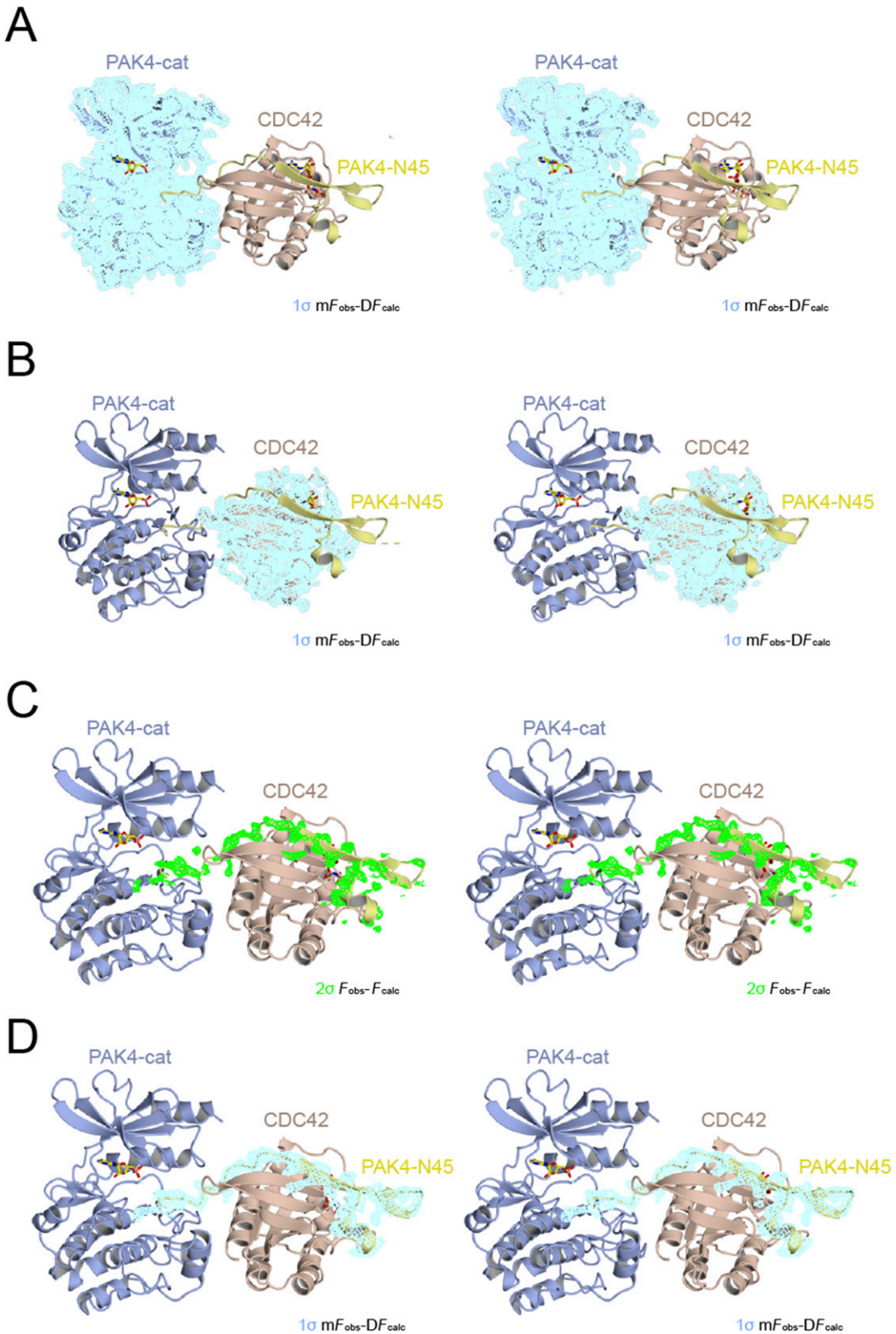

Fig. S3. Crystal structure of PAK4^{cat}-PAK4^{N45}-CDC42. (*A*) Stereo views showing the refined electron density map (mF_{obs} – DF_{calc} contoured at 1.0 σ) of PAK4 catalytic domain and (*B*) the small GTPase, CDC42. (*C*) Unbiased electron density map (F_{obs} – F_{calc} contoured at 2.0 σ) showing strong density for PAK4^{N45}. (*D*) Final refined electron density map (mF_{obs} – DF_{calc} contoured at 1.0 σ) showing strong density for PAK4^{N45}.

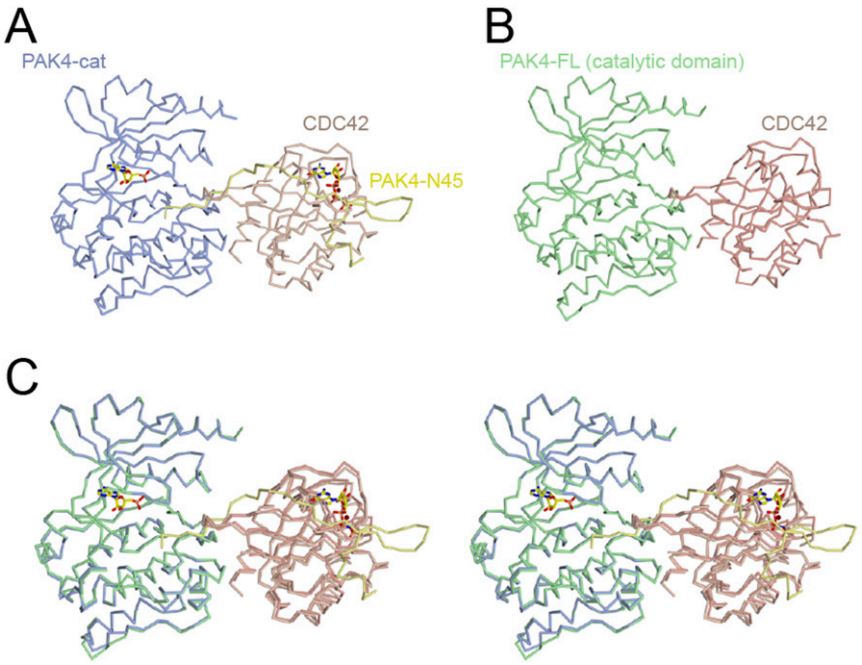

Fig. S4. Comparison of PAK4^{FL}-CDC42 and PAK4^{cat}-PAK4^{N45}-CDC42 structures. (*A*) Ribbon diagram of refined PAK4^{cat}-PAK4^{N45}-CDC42 structure. (*B*) Ribbon diagram of PAK4^{FL}-CDC42 molecular replacement solution. (*C*) Stereo view of the superposition of the two structures. Superposition is conducted for the kinase domain C-lobes only, as this accentuates any differences.

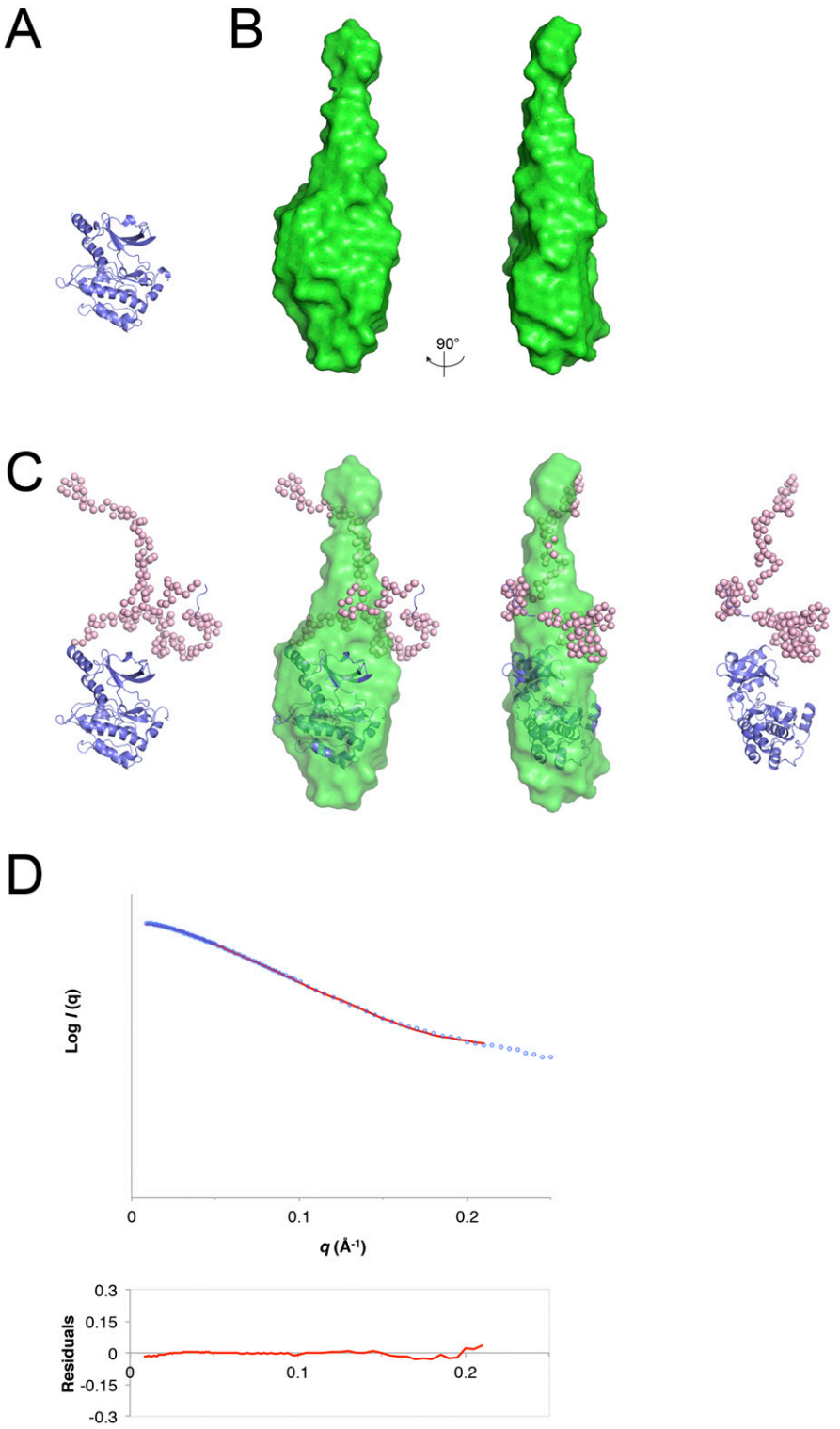

Fig. S5. SAXS analysis and rigid body modeling for PAK4-FL. (*A*) Crystal structure of PAK4^{cat} in blue. (*B*) Averaged SAXS molecular envelope generated using DAMMIF (DAMFILT envelopes shown) for PAK4^{FL}. (*C*) Rigid body analysis. CORAL model of PAK4^{FL} with the best statistical fit to the experimental data. Interdomain dummy atoms are shown as pink spheres. Superposition with the DAMMIF envelope is shown in the central pair. (*D*) Rigid body analysis. Experimental SAXS data (logarithmic scale) are shown fitted to the theoretical scattering profile of the best rigid body (red line). Residuals are shown below.

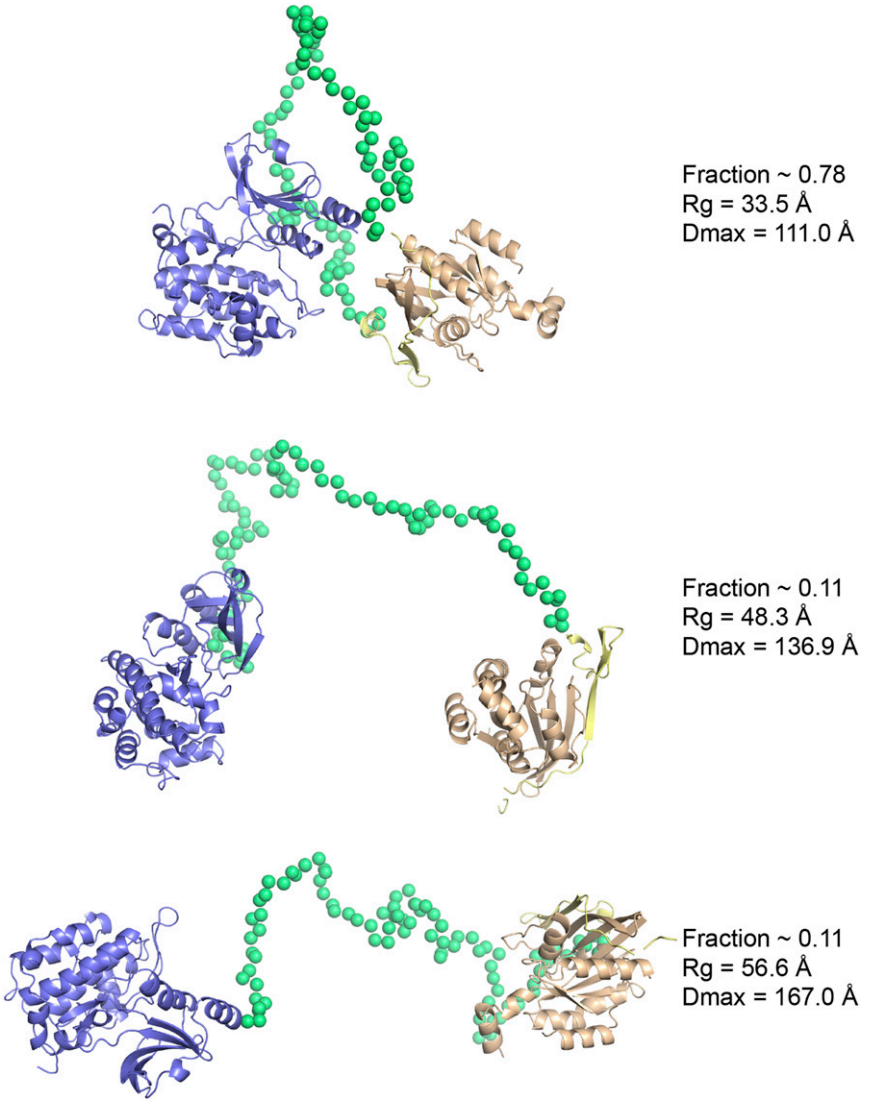

Fig. S6. Composition of the best EOM ensemble model. Three PDB models of PAK4-CDC42 were used in the best EOM model, these are shown, with the fraction comprised in the model, the R_g and D_{max} for each PDB model. As the complex in solution is flexible, this composition corresponds to the best fit to the experimental data under the parameters used.

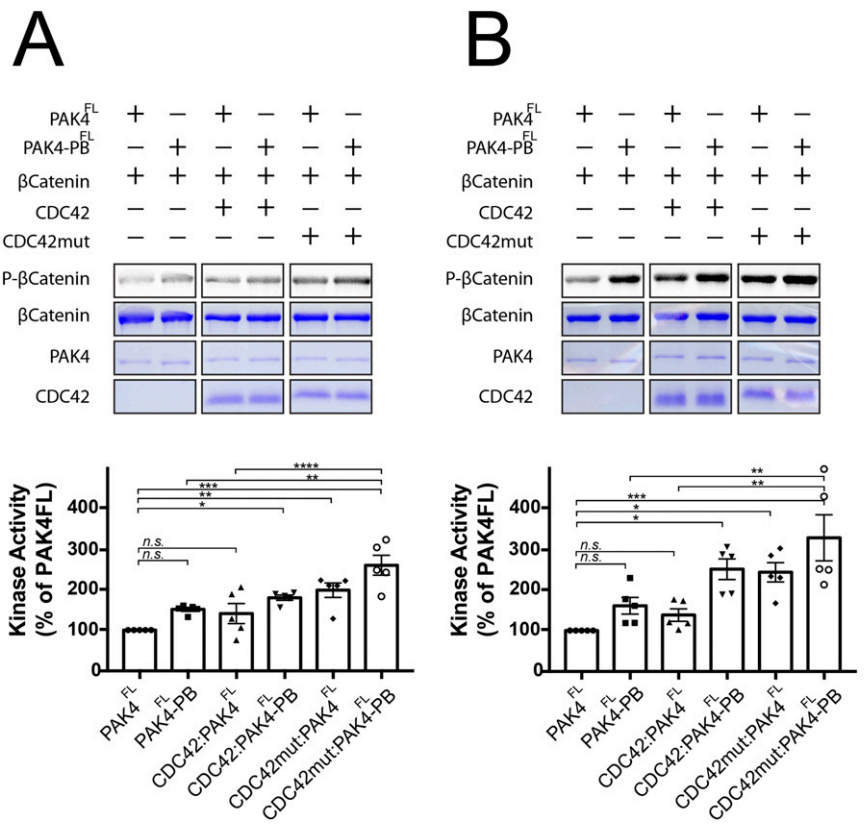

Fig. S7. In vitro kinase assay. In vitro kinase assays using purified PAK4^{FL} or PAK4^{FL} mutated in its polybasic region (R5A/R8A), PAK4^{FL}-PB. Assays were incubated with either CDC42 (Q61L, constitutively active mutant) or CDC42mut (Q61L, E171R, L174R, and E178R). Full-length β-catenin was added as the substrate and kinase activity monitored by autoradiography. Two time points monitored are 5 min (*A*) and 10 min (*B*). $n = 5$. Bar charts show activities as a percentage of PAK4^{FL} activity. ****$P < 0.0001$, ***$P < 0.002$, **$P < 0.02$, *$P < 0.03$, and *n.s.* means not significant.

Table S1. SAXS data collection and refinement statistics

	$PAK4^{FL}$	$PAK4^{FL}$-CDC42
Data collection parameters		
Beamline	NSLS-II LiX	NSLS-II LiX
Beam geometry	300- × 300-μm point source	300- × 300-μm point source
Detector	Pilatus 1M	Pilatus 1M
Beam wavelength, eV	10,790	10,790
Temperature, K	295	295
Protein concentration, mg/mL	11.7/5.9/3.0	6.3/3.1/1.6
Q range, $Å^{-1}$	0.009–0.244/0.009–0.253/0.009–0.256	0.009–0.256/0.009–0.256/0.009–0.256
No. of exposures	5/5/5	5/5/5
No. of exposures averaged	5/5/5	5/5/5
Exposure time, s	5/5/5	5/5/5
Structural parameters		
$I(0)$, cm^{-1} (reciprocal)	50.5/23.1/11.0	54.9/26.3/12.6
R_g, Å (reciprocal)	38.2/36.2/36.9	39.4/37.4/38.2
$I(0)$, cm^{-1} (real)	50.5 ± 0.8/23.1 ± 0.7/11.0 ± 0.6	54.9 ± 0.8/26.3 ± 0.8/12.6 ± 0.8
R_g, Å (real)	38.5 ± 1.4/36.5 ± 2.6/37.3 ± 4.4	39.6 ± 1.3/37.6 ± 2.8/38.5 ± 5.9
D_{max}, Å	172/172/171	169/170/173
Model building		
Theoretical molecular mass, kDa	50.9	71.8
Porod volume	86,294	106,337
Molecular mass from Porod volume, kDa	50.7	62.5
No. of ab initio models calculated	20	20
Best model *P* value*	0.0088	0.0055
Best adjusted model *P* value*	0.1865	0.1164
Molecular mass from excluded volume, kDa	56.7	77.9
Rigid body model best χ^2 value	0.42	0.83
EOM ensemble χ^2 value	n.d.	0.13
EOM ensemble R_g, Å	n.d.	37.8
Software		
Data reduction and averaging	pyXS	pyXS
Data processing	Primus	Primus
Ab initio model generation	DAMMIF	DAMMIF
Rigid body model	CORAL	CORAL
Interdomain flexibility	EOM	EOM
Three-dimensional graphics representation	Pymol	Pymol

n.d., not determined.
*CorMap *P* values from DAMMIF.

Table S2. Crystallographic data collection and refinement statistics

	Cocrystallized complex	
	$PAK4^{cat}$-$PAK4^{N45}$-CDC42	$PAK4^{FL}$-CDC42
PDB ID code	5UPK	5UPL
Data collection		
Space group	$P2_1$	$P6_3$
X-ray source and detector	APS 24-ID-E ADSC Q315	APS 24-ID-E ADSC Q315
Wavelength, Å	0.97920	0.97922
Unit cell		
a, b, c, Å	58.5, 61.6, 85.8	141.7, 141.7, 62.1
α, β, γ, °	90, 91.6, 90	90, 90, 120
Resolution range,* Å	50.00–2.40 (2.49–2.40)	50.00–3.00 (3.11–3.00)
No. of unique reflections	24,144	14,433
Completeness,* %	100 (100)	99.9 (100)
R_{pim},* %	7.4 (91.2)	3.4 (70.7)
$CC_{0.5}$, % (in high-resolution bin)	31.1	58.8
Mean $<I>/<\sigma I>$*	12.0 (1.8)	20.3 (1.6)
Wilson *B*-factor	47.3	77.2
Redundancy	10.9 (10.6)	18.0 (17.2)
Refinement statistics		
Resolution range,* Å	50.0–2.4 (2.46–2.4)	43.6–3.0 (3.23–3.0)
R_{factor},* %	22.1 (22.9)	25.2(36.3)
Free R_{factor},* %	26.4 (32.1)	30.1 (47.3)
Free *R* reflections,* %	4.6 (4.1)	5.0 (4.7)
Free *R* reflections,* no.	1,097 (68)	726 (129)
Residues built		
PAK4	5–43, 300–588	299–589
CDC42	2–133, 137–177	2–178
No. of water molecules	25	1
Mean *B*-factor, $Å^2$		
Protein (PAK4)	60.6	73.4
Protein ($PAK4^{cat}$)	56.2	—
Protein ($PAK4^{N45}$)	88.8	—
AMP-PNP	62.9	—
Protein (CDC42)	84.2	218.7
GMP-PNP	83.9	—
Mg^{2+}	76.6	—
H_20	48.6	—
Model statistics		
Rmsd bond lengths, Å	0.008	0.012
Rmsd bond angles, °	1.375	1.557
Ramachandran plot, % (favored/allowed/disallowed)	96.4/3.6/0	95.4/4.1/0.4

*Indicates high-resolution shell.

Table S3. Thermodynamic properties of the interaction between PAK4 and small GTPases RAC1 and CDC42

Sample cell	Syringe	K_d, μM	N	ΔH, kJ/mol	ΔS, J/mol·K	ΔG, kJ/mol
$PAK4^{FL}$	CDC42	0.2	0.91	−81.2	−145.1	−37.9
$PAK4^{FL}$	CDC42	0.5	0.95	−81.6	−152.4	−36.2
$PAK4^{FL}$	$CDC42^{ELE\text{-}RRR}$	1.0	0.92	−91.2	−191.1	−34.3
$PAK4^{FL}$	$CDC42^{ELE\text{-}RRR}$	1.1	0.88	−100.0	−211.5	−37.0
$PAK4^{FL}$	RAC1	3.2	1.29	−38.5	−24.0	−31.3
$PAK4^{FL}$	RAC1	2.8	0.70	−40.8	−30.7	−31.7
$PAK4^{cat}$	$PAK4^{N45}$:CDC42	142.0	1.18	14.3	121.7	−21.9
$PAK4^{cat}$	$PAK4^{N45}$:CDC42	66.7	1.51	12.4	121.6	−23.8
CDC42	$PAK4^{N45}$	0.98	0.60	−103.9	−232.7	−34.55
CDC42	$PAK4^{N45}$	1.43	0.53	−96.52	−211.8	−33.36
CDC42	$PAK4^{N45}$	1.58	0.56	−102.4	−232.3	−33.11
RAC1	$PAK4^{N45}$	7.7	0.82	−101.2	−241.7	−29.18
RAC1	$PAK4^{N45}$	12.5	0.90	−111.1	−278.7	−28.00
$PAK4^{FL\text{-}R489A}$	CDC42	1.58	0.69	−59.37	−88.04	−33.12
$PAK4^{FL\text{-}R489A}$	CDC42	1.60	1.33	−116.2	−278.9	−33.08
$PAK4^{FL\text{-}R489A}$	CDC42	0.71	1.04	−56.21	−70.87	−35.08
$PAK4^{cat}$	$PAK4^{N45}$	No heat	No heat	No heat	No heat	No heat

Data from each of the independent ITC experiments are shown. Experiments conducted at 298 K. No heat indicates no measurable heat was observed from the titration.